




Identifying Key Driving Processes of Major Recent Heat Waves

Journal Article

Author(s):

Wehrli, Kathrin ; Guillod, Benoit P.; Hauser, Mathias ; Leclair, Matthieu; Seneviratne, Sonia I. 

Publication date:

2019-11-27

Permanent link:

<https://doi.org/10.3929/ethz-b-000381735>

Rights / license:

[Creative Commons Attribution-NonCommercial-NoDerivatives 4.0 International](#)

Originally published in:

Journal of Geophysical Research: Atmospheres 124(22), <https://doi.org/10.1029/2019JD030635>

Funding acknowledgement:

617518 - Land-Climate Interactions: Constraints for Droughts and Heatwaves in a Changing Climate (EC)



RESEARCH ARTICLE

10.1029/2019JD030635

Key Points:

- Observed temperature anomalies are well reproduced in a climate model when constrained by observed atmospheric circulation and soil moisture
- In these constrained runs soil moisture and atmospheric circulation are equally important for temperature anomalies of five recent heat waves
- Disentangling the physical drivers for the five investigated heat waves reveals a warming signal over the recent decades

Supporting Information:

- Supporting Information S1

Correspondence to:

K. Wehrli,
kathrin.wehrli@env.ethz.ch

Citation:

Wehrli, K., Guillod, B. P., Hauser, M., Leclair, M., & Seneviratne, S. I. (2019). Identifying key driving processes of major recent heat waves. *Journal of Geophysical Research: Atmospheres*, 124, 11,746–11,765. <https://doi.org/10.1029/2019JD030635>

Received 13 MAR 2019

Accepted 11 OCT 2019

Accepted article online 1 NOV 2019

Published online 19 NOV 2019

Corrected 10 DEC 2019

This article was corrected on 10 DEC 2019. See the end of the full text for details.

©2019. The Authors.

This is an open access article under the terms of the Creative Commons Attribution-NonCommercial-NoDerivs License, which permits use and distribution in any medium, provided the original work is properly cited, the use is non-commercial and no modifications or adaptations are made.

Identifying Key Driving Processes of Major Recent Heat Waves

Kathrin Wehrli¹ , Benoit P. Guillod^{1,2} , Mathias Hauser¹ , Matthieu Leclair¹ , and Sonia I. Seneviratne¹

¹Institute for Atmospheric and Climate Science, Department of Environmental Systems Science, ETH Zurich, Zurich, Switzerland, ²Institute for Environmental Decisions, Department of Environmental Systems Science, ETH Zurich, Zurich, Switzerland

Abstract Heat waves lead to major impacts on human health, food production, and ecosystems. To assess their predictability and how they are projected to change under global warming, it is crucial to improve our understanding of the underlying processes affecting their occurrence and intensity under present-day climate conditions. Beside greenhouse gas forcing, processes in the different components of the climate system—in particular the land surface, atmospheric circulation, and the oceans—may play a key role in changing the odds for a particular event. This study aims to identify the role of the individual drivers for five heat waves (and, in some cases, of concurrent droughts) in the recent decade. Simulations are performed with the Community Earth System Model using nudging of horizontal atmospheric circulation and prescription of soil moisture. The fully constrained model accurately reproduces how anomalous an event was. Factorial experiments, which force the model toward observations for one or several key components at a time, allow us to identify how much of the observed temperature anomaly of each event can be attributed to each driver. Considering all analyzed events, atmospheric circulation and soil moisture play similarly important roles, each contributing between 20% and 70% to the events' anomalies. This highlights that the role of thermodynamics can be just as important as that of the dynamics for temperature extremes, a possibly underestimated feature. In addition, recent climate change amplified the events and contributed between 10% and 40% of the events' anomalies.

1. Introduction

The recent decade has seen a variety of extreme heat events, some of which led to considerable impacts on agriculture, economy, and society. Extreme conditions may result from the contribution of a single driving mechanism as well as from the interplay of several drivers and processes. We distinguish here three main physical drivers for land-based heat waves: (1) atmospheric circulation, (2) land surface conditions, and (3) sea surface temperatures (SSTs). In addition, there is well-established evidence that greenhouse gas (GHG) forcing affects not only the mean climate state but also climate variability, and the likelihood and intensity of weather and climate extremes (Donat et al., 2013; Fischer & Knutti, 2015; Power & Delage, 2019; Seneviratne et al., 2012). To improve forecasts and constrain projections, we need to better understand these contributing factors, that is, the driving physical mechanisms under present-day climate conditions.

The likelihood of extreme events has changed since preindustrial times due to climate change mainly induced by anthropogenic GHGs and to a smaller extent also due to land-use and land cover change (Deo et al., 2009; Donat et al., 2013; Fischer & Knutti, 2015; Lejeune et al., 2018; Seneviratne et al., 2012; Thiery et al., 2017). There is no deterministic answer to the question of whether climate change was the cause of a specific event. It is, however, possible to assess and quantify the contribution of different factors to a change in the odds of the event or a class of events (e.g., Hauser et al., 2016; Hope et al., 2015; Schaller et al., 2016). Early studies on extreme events used a probabilistic attribution approach to determine the change in likelihood resulting from GHG forcing (Shepherd, 2016). This approach requires the comparison of a “factual” and a “counterfactual” probability for a class of events (e.g., Otto et al., 2012; Stott et al., 2004). In contrast, a newer but complementary approach is based on “storylines.” It seeks the best estimate of the contribution of anthropogenic forcing for a particular event and identifies a chain of factors leading to this event in order to assess the role of each (Shepherd, 2016; Trenberth et al., 2015). This latter framework can also be expanded to consider the attribution of extreme events to different atmospheric, oceanic, and land

conditions, in a more mechanistic perspective (as in, e.g., Arblaster et al., 2014; Hauser et al., 2016; Hope et al., 2015; Wang et al., 2016).

The ocean is a major driver of climate variability (Brönnimann, 2007). Anomalies in the SSTs can influence local weather and climate through modifications of the atmospheric flow and can also have remote effects, so-called teleconnections. SST anomalies associated with climate phenomena such as the El Niño Southern Oscillation (ENSO; e.g., Ropelewski & Halpert, 1987; Su et al., 2001) are related to temperature and precipitation anomalies all over the globe (e.g., Hoell et al., 2017; Kushnir et al., 2010; Power et al., 1999; Schubert et al., 2009; Su et al., 2001). For northern Eurasia it has been suggested that certain SST patterns can increase heat wave risk by modifying the atmospheric circulation (e.g., Schubert et al., 2014). However, SSTs may play a weaker role in some events; for instance no clear role was identified in the case of the 2010 Russian heat wave (Dole et al., 2011; Hauser et al., 2016).

Heat waves are often found to be linked to anomalies of the atmospheric flow (Meehl & Tebaldi, 2004; Parker et al., 2014; Pfahl & Wernli, 2012). It was shown that in the northern midlatitudes hot extremes are often related to persistent anticyclones (e.g., Pfahl & Wernli, 2012; Schubert et al., 2014). Quinting and Reeder (2017) similarly find that heat waves in southeastern Australia are often related to anticyclones. These anticyclones could be driven by the ocean conditions, as suggested above, but can also result from internal variability of the atmospheric circulation.

Land surface feedbacks associated with soil moisture (SM) availability can play an important role in amplifying hot extremes, especially in a warming climate (e.g., Hirschi et al., 2011; Mueller & Seneviratne, 2012; Seneviratne et al., 2006, 2010, 2013; Vogel et al., 2017). Limited SM can enhance heat waves by a reduction in evaporative cooling (Fischer et al., 2007; Seneviratne et al., 2006, 2010) and prolong the event duration due to SM memory (e.g., Lorenz et al., 2010) and feedbacks with the atmospheric boundary layer (Miralles et al., 2014). Severe heat waves are often found to co-occur with droughts, especially in transitional climate regions, which is a consequence of the strong land-atmosphere coupling in these regions (Zscheischler & Seneviratne, 2017).

A better understanding of the interplay of the processes driving a specific extreme event and their relative importance can be attempted through observation-based studies. This is, however, generally difficult due to the nonlinear interactions and manifold processes involved, as well as due to the short observational record available for many types of extremes. Arblaster et al. (2014), Hope et al. (2015), and Wang et al. (2016), for example, used multiple linear regression in observations to disentangle the role of large-scale climate drivers and SM for heat waves. The impact of the observed initial conditions can be determined in forecast sensitivity experiments as in Arblaster et al. (2014) and Hope et al. (2016). Another way to disentangle the role of the drivers to single events is to constrain one (or several) of them in climate model simulations (Fischer et al., 2007; Hauser et al., 2016; Jaeger & Seneviratne, 2011).

Here, we perform simulations with the Community Earth System Model (CESM; Hurrell et al., 2013). SSTs are prescribed to quantify their role for various events. To prescribe the atmospheric circulation, we use a nudging approach (Jeuken et al., 1996), which allows us to study the dynamic contribution in isolation. In a second set of experiments, we condition on the state of the land surface by using SM prescription (Koster et al., 2004). Within this framework we can quantitatively estimate the contributions of the atmospheric dynamics and the land surface as well as the role of the ocean and of recent climate change. We choose five recent heat waves that occurred between 2010 and 2016 in different continents of the world. Each event received attention in the media, owing to drastic consequences such as damage caused to food production, severe wildfires, and increased mortality. In chronological order the events investigated are as follows: the 2010 Russian heat wave, an extremely long-lasting heat wave with record-breaking temperatures in large areas in Eastern Europe; the 2012 Midwest heat wave, which hit the United States simultaneously with a record drought; the 2012/2013 Australian heat wave, which started out as a meteorological drought but developed into a heat wave; the 2015 European heat wave, a sequence of heat waves co-occurring with an unprecedented rainfall deficit; and the 2015/2016 South African heat wave, which was associated with sudden drought conditions. The results presented herein shall contribute to increased understanding of the main factors driving these record events. In the following, we will first give an overview of the model used, and the experiments run and introduce the data sets and analysis strategy (section 2). In section 3 we validate the SM prescription (section 3.1), review literature on the investigated events, and then present and discuss

our results for each event, first separately (section 3.2) and then in a synthesized assessment (section 3.3). We conclude and reflect on the analysis methodology in section 4.

2. Model and Methods

We conduct global climate model simulations with CESM Version 1.2 (Hurrell et al., 2013) for the period 1979 to 2016. CESM couples the Community Atmosphere Model Version 5.3 (CAM5; Neale et al., 2012) and the Community Land Model version 4 (CLM4; Lawrence et al., 2011; Oleson et al., 2010), which are both run on $0.9^\circ \times 1.25^\circ$ horizontal resolution. In the vertical dimension there are 30 layers up to 2 hPa for the atmosphere and 10 soil layers with active hydrology down to 3.8 m for the land component. SSTs and sea ice fractions are prescribed using transient monthly observations (Hurrell et al., 2008). Solar forcing follows historic data until the end of 2005; thereafter, we use Coupled Model Intercomparison Project Phase 6 (CMIP6) solar forcing (observations for 2006–2014 and forecast from 2015; see Matthes et al., 2017). The atmospheric chemistry, aerosols, and land-use change follow the representative concentration pathway 8.5 (RCP8.5; van Vuuren et al., 2011) scenario after 2005. GHGs follow CMIP5 recommendations for 20th century simulation until 2005. From 2006 until the end of the simulation period (December 2016) they are prescribed from observed sources for CO_2 , CH_4 , N_2O , and from RCP8.5 scenario data for other GHGs. The observed global mean values of CO_2 , CH_4 , and N_2O were obtained from the National Oceanic and Atmospheric Administration (NOAA; CO_2 : Dlugokencky & Tans, 2018; CH_4 : Dlugokencky, 2018; and N_2O : NOAA Earth System Research Laboratory, 2018).

2.1. Atmospheric Nudging

Through atmospheric nudging, we aim to control the large-scale circulation in the model, following the same approach as in Wehrli et al. (2018). To this end, we relax the horizontal winds toward observations (similarly to Kooperman et al., 2012; Zhang et al., 2014). We use a height-dependent nudging, such that the large-scale circulation in the upper atmosphere is forced to follow the observations (mostly above 700 hPa), whereas the nudging strength is zero at the surface and thus the boundary layer can evolve freely (see Wehrli et al., 2018, for the profile). This allows for interaction between land and atmosphere (i.e., surface climate and winds) through surface turbulent fluxes. The target fields for the nudging are retrieved from 6-hourly zonal and meridional winds from the ERA-Interim reanalysis (Dee et al., 2011). The approach is described in detail and validated in Wehrli et al. (2018).

2.2. SM Prescription

To quantify the effect of soil water availability on each event, we perform simulations where we prescribe SM. The employed SM prescription module for CLM4 was developed and evaluated by Hauser et al. (2017). The hydrology is computed actively in the model, but at the end of each time step SM is overwritten by a target value. We prescribe SM to (a) pseudo-observations and (b) the 1982–2008 climatology (i.e., repeated mean seasonal cycle) of these pseudo-observations. The pseudo-observations are generated using the land model, CLM4, in off-line mode forced by ERA-Interim atmospheric fields to produce daily SM fields. This is necessary because SM as simulated by a land surface model is inherently dependent on the employed model, not only due to differences in the parameterized soil properties but also due to different model climatologies (Koster et al., 2009). The direct transfer of SM between models and from observational products to models can thus lead to fundamental and deleterious inconsistencies. Using pseudo-observations overcomes these problems, and the produced SM fields are consistent with the employed land model. SM is only prescribed if the soil temperature in the model is above freezing. The soil liquid water is set to the total SM of the target data set, that is, the sum of soil liquid and soil ice. In the case of soil temperatures below 0°C the model interactively computes the soil ice and water content. The advantage over an approach that prescribes soil ice is that the model does not artificially create ice, which can result in an unrealistic ground heat flux from the melting of that ice (Hauser et al., 2017). Thus, the simulations with prescribed SM have exactly the same soil water content as the pseudo-observations, except when parts of the soil are at subzero temperatures (not shown). We find only small differences between pseudo-observations derived with a different atmospheric forcing data set (Text S1 and Figure S4 in the supporting information).

2.3. Reanalysis and Observation-Based Data Sets

We use a number of reanalysis and observational data sets to evaluate our simulations. Our main reference data set is ERA-Interim, since the model is forced based on this data set in the constrained simulations.

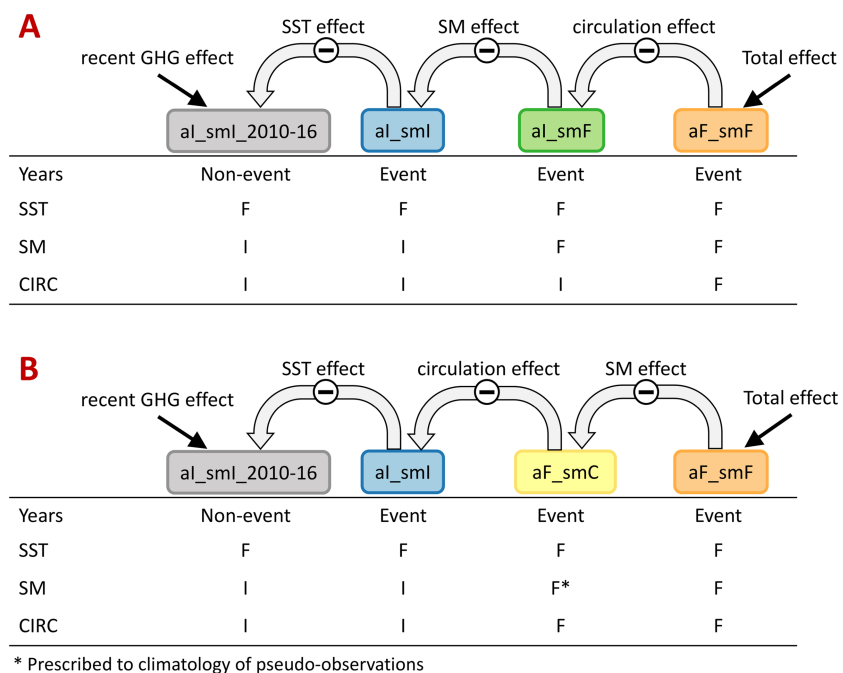


Figure 1. Schematic overview of model ensembles and effects isolated. In all cases, the anomaly relative to the 1982–2008 climatology is considered. Forced components are indicated by “F” and interactive components by “I”. The atmospheric circulation (CIRC) is forced by applying a nudging of the horizontal winds toward ERA-Interim. Soil moisture (SM) is forced by prescribing pseudo-observations. Sea surface temperatures (SSTs) are forced with transient monthly observations (section 2). *aI_smI_2010-16* refers to the years 2010–2016 of *aI_smI* (only nonevent years), while in all other cases, only the event year is considered. The effects are computed by taking differences along the arrows as indicated by the minus sign. The two approaches marked by the red letters A and B differ in how SM effects are separated from circulation effects.

For SM we show data from ERA-Land, which corresponds to ERA-Interim/Land (Balsamo et al., 2015), but without precipitation correction. ERA-Land was shown to have good agreement with in situ SM observations (Rodríguez-Fernández et al., 2016).

We further compare our results to observation-based estimates. For temperature we use gridded daily maximum temperatures from Berkeley Earth (Rohde, Muller, Jacobsen, Muller, et al., 2013; Rohde, Muller, Jacobsen, Perlmutter, et al., 2013). For precipitation we show data from the Multi-Source Weighted-Ensemble Precipitation data set, Version 2.2 (MSWEP; Beck et al., 2018) and the full data product from the Global Precipitation Climatology Centre, Version 2018 (GPCC; Ziese et al., 2018). We compare incoming shortwave radiation (SW_{in}) to the SYN1deg satellite product Version 4a by the Clouds and the Earth’s Radiant Energy System project (CERES; Doelling, 2017).

We validate the ERA-Interim surface turbulent fluxes of latent heat (LH) and sensible heat (SH) against data from the Global Soil Wetness Project 2 (GSWP-2; Dirmeyer et al., 2006; see Figure S1). To validate the SM pseudo-observations, we use the following observational products: The combined active and passive SM product v04.4 from the European Space Agency Climate Change Initiative (ESA-CCI; Dorigo et al., 2017; Gruber et al., 2017; Liu et al., 2012); global mass concentration blocks from the Gravity Recovery and Climate Experiment (GRACE; Watkins et al., 2015; Wiese et al., 2016, 2018); and WFDEI atmospheric forcing from the WATER and global CHange project (WATCH-WFDEI; Weedon et al., 2014, 2011).

2.4. Experiments

We perform four experiments that all use prescribed ocean temperatures but differ in whether the SM and/or the atmospheric circulation are prescribed or interactive. To isolate the contribution of the different considered drivers to the events, the first three experiments are progressively forced toward observations (Figure 1). In the first experiment (*aI_smI*) we prescribe ocean temperatures only; in the second experiment (*aI_smF*), we prescribe SSTs and SM toward observations; and in the third experiment (*aF_smF*), we additionally nudge the atmosphere. We do not run an experiment with nudged atmosphere and interactive SM

because nudging the large-scale circulation in isolation also constrains SM (and, hence, land-atmosphere interactions) similarly to the case where both are prescribed. Therefore, to assess the influence of the atmospheric circulation without the effect of that year's SM, we have designed a fourth experiment (*aF_smC*), where the atmosphere is nudged and SM conditions are prescribed to the 1982–2008 climatology of the pseudo-observations (section 2.2).

All experiments cover the years 1979 to the end of 2016. The first 3 years are used as spin-up time, and the years 1982–2008 are used to create a baseline (called climatology in the following). The effect of recent climate change is estimated from the climatology of each experiment. The ensemble size over that period is five members for the experiments with interactive atmosphere and one member for the experiments with nudged atmosphere, as there is only negligible variability between ensemble members due to nudging. In 2009, the *aI_smI* and *aI_smF* experiments are enlarged to a total of 100 ensemble members by creating 19 additional members from each original member through the application of a perturbation of the temperature field (Kay et al., 2015). To allow ensemble members to diverge the year 2009 is regarded as spin-up, and events of the years 2010–2016 are considered in the analysis.

2.5. Data Analysis

To make the considered heat waves better comparable between the experiments and to focus on their respective severity, we compute anomalies from the climatology of the analyzed variable. The climatologies of SM, temperature, precipitation, and connected variables show differences between the experiments even though the global mean temperature is very similar (not shown). This arises from the prescription methodologies. For example, in the annual climatological mean soils in Australia are drier in the experiments with prescribed SM, while eastern Europe and Russia are generally wetter, especially in summer and fall (Figure S2). This affects surface temperature due to a different amount of moisture available for LH fluxes. Similarly, the atmospheric nudging does not only alter the timing and characteristics of a specific weather pattern but also induces changes in the climatology of the large-scale circulation, such as changes to the path and frequency of pressure systems and some of the precipitation patterns, which again results in a different climatology of temperature (Wehrli et al., 2018). Using anomalies relative to the experiment's own climatology mitigates these effects, hence allowing us to identify the contributions of the components to each event.

To validate surface SM, we compare ESA-CCI to the accumulated liquid and ice water content of the upper 45 mm in the pseudo-observations. We regrid the SM pseudo-observations to the spatial resolution of ESA-CCI (0.25°). All grid points for all time steps that are not available in the satellite product are masked out. Thus, some regions are less well sampled than others due to dense vegetation or snow. Surface SM is then standardized (and hence deseasonalized) by the daily mean and standard deviation of the smoothed (15-day running mean) climatology over 1995–2016. This allows us to compare SM data sets from different sources (Koster et al., 2009). We compute correlations of the standardized surface SM between ESA-CCI and the pseudo-observations. For the validation of total water storage we retrieve the surface mass change on the Jet Propulsion Laboratory (JPL) mass concentration blocks (mascons) from GRACE. For the model we compute the total water storage and remove the 2004–2009 mean, as is done for GRACE. Then we regrid to 0.5° resolution and average to the footprint of each mascon. Total water storage from GRACE and the pseudo-observations is deseasonalized relative to 2004–2009.

The events are analyzed by taking spatial averages over a region, whose extent is taken from literature. The analysis excludes ocean grid points. For each event we focus on the 31-day period during which the event was most extreme. To define this event period, we use near-surface temperatures from ERA-Interim and look for the 31 hottest consecutive days for the defined region and the event year (for the events on the Southern Hemisphere the event year is defined from July to June to encompass the entire summer season from December to February). We examine daily maximum temperature (TX), daily mean precipitation, SM, Evaporative Fraction (EF), 500-hPa Geopotential height, and SW_{in} , all averaged over the 31-day event period. We compute SM accumulated in the upper 1 m of the soil and standardize it with respect to 1982–2008, the same way as for surface SM. We compute EF from LH and SH as $\frac{LH}{LH+SH}$.

Note that, unlike in classical event attribution, we partly rely on existing literature to define the event instead of using thresholds (i.e., for the choice of the year investigated). Also, because nudging leads to one realization of the event, only the “mean” can be investigated. Hence, since we analyze the ensemble mean and full range of ensemble members (for the nonnudged simulations), we follow a rather conservative approach to analyze extreme events.

2.6. Disentangling the Contributions to the Event Anomaly

In this study we want to disentangle the contributions of different physical drivers (recent climate change, the ocean state, SM, and atmospheric circulation) to the event magnitude for temperature. Thereby, we assume that the different contributions are additive. In our framework, the anomaly in aF_smF corresponds to the event as simulated in the model (100%). We assess the effect of the various factors as follows (Figure 1): First, the contribution of recent climate change is estimated as the mean anomaly of the years 2010–2016 of aI_smI relative to its climatology (1982–2008). We call the resulting anomaly $aI_smI_{2010-16}$, and—as the particular year of the event is always excluded—it has 6×100 values (6 years; 100 ensemble members). This period includes the La Niña events of 2010/2011 and 2011/2012 as well as the El Niño events of 2014/2015 and 2015/2016. Thus, we do not expect a bias toward one of the phases of ENSO. Although the variability in the ocean is limited, the interactive atmosphere allows for variability between the 600 members. Therefore, we assume that it is possible to estimate the recent climate forcing independently of a particular SST pattern. We refer to this as the recent GHG effect; however, aerosol effects might play an important role as well. Note that this does not correspond to the total climate change signal since preindustrial times (which is expected to be larger), as it is only relative to a recent climatology (1982–2008). Second, to identify the signal of the different climate drivers, we form differences between the experiments. This was done similarly for the ocean by Lim et al. (2016) in a seasonal forecast sensitivity study. The anomaly in aI_smI combines both the ocean-induced effect and the recent GHG forcing. Hence, the contribution of SSTs of the event year is estimated by subtracting the contemporaneous anomalies, which include recent GHG forcing: $aI_smI - aI_smI_{2010-16}$. In doing so, we assess if SSTs of the particular event year led to warmer or colder event temperatures in comparison to the nonevent years in 2010–2016. Finally, there are two approaches to estimate the effects of SM and atmospheric circulation (Figure 1):

- A. The effect of SM is quantified as $aI_smF - aI_smI$. That is, we isolate the SM effect by subtracting the contributions from SSTs and recent GHG forcing from the event anomaly given the SM, SST, and GHGs. Note that this may include indirect SM effects onto circulation. The circulation effect (given the event's SM) is given by $aF_smF - aI_smF$. This corresponds to the total event anomaly minus the combined contribution of SM, SSTs, and recent GHG forcing for the event year.
- B. The effect of SM (given the event's atmospheric circulation) is quantified as $aF_smF - aF_smC$, which corresponds to the total event anomaly minus the contributions of the event circulation on a climatological SM year, the ocean-induced effects, and recent GHG forcing. The circulation effect is quantified by $aF_smC - aI_smI$. That is we subtract the contributions from SSTs and recent GHG forcing from the event anomaly given the circulation and a climatological SM year.

3. Results and Discussion

In the following, we first evaluate the SM pseudo-observations in section 3.1. Then we examine five extreme heat waves in different regions of the world (left panels in Figure 3) with the aim to distinguish the individual drivers. Where relevant, we further expand our discussion to concurrent drought conditions. In section 3.2 we examine each event individually and describe their evolution and characteristics. Section 3.3 gives a synthesis of the main drivers of temperature anomalies for all events.

3.1. Evaluation of SM Pseudo-Observations

We validate the pseudo-observations against satellite products for surface SM and total water storage (section 2.5). Overall, the pseudo-observations perform well compared to the satellite data (Figure 2). During the event period, both satellite and pseudo-observations show dry soil conditions that were among the lowest observed for the time period shown. The surface SM anomaly correlation between ESA-CCI and the pseudo-observations is 0.37 for the weighted global average (Figure 2a). Correlations are generally higher for the considered event regions (Russia: 0.48, Europe: 0.49, Midwest: 0.49, Australia: 0.67, South Africa: 0.48). Lower correlations are found mainly for regions with frozen soil or regions that are covered with snow or dense vegetation for most of the year, which poses a challenge for microwave remote sensing (de Jeu et al., 2008; Seneviratne et al., 2010). Correlations are also lower for mountainous regions (Alps and Himalaya), which could be related either to issues with resolving heterogeneous SM patterns in CLM4 or to reduced reliability of the satellite data over the partly frozen and snow-covered soil. The temporal evolution of surface SM during the year of the event is well captured by the pseudo-observations for the 2010 Russian heat

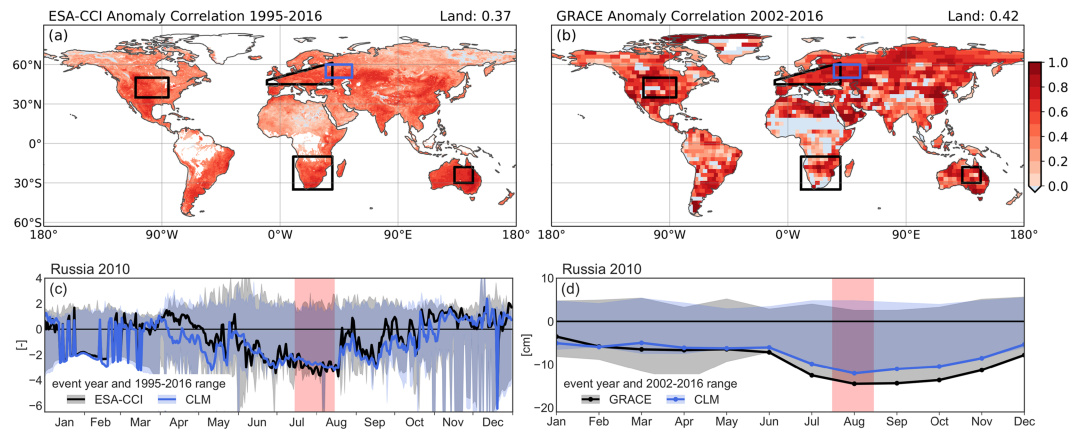


Figure 2. Validation of the SM pseudo-observations. (a) Anomaly correlation of standardized surface SM between pseudo-observations and ESA-CCI for 1995–2016. The blue rectangle marks the region of the Russian heat wave; the black shapes mark the other event regions. (b) Same but for total water storage anomalies relative to 2004–2009 (deseasonalized), shown for the years 2002–2016 and taking GRACE as reference. (c) Surface SM evolution for the Russian heat wave 2010; the gray and blue shadings show the range for 1995–2016. The red shading marks the event period. (d) Same but for total water storage anomalies (deseasonalized). For validation of the other regions see Figure S5.

wave (Figure 2c) as well as for the other events (Text S2; Figure S5). The time series for surface SM shows large short-term variability, which is likely related to the thin surface layer and to missing data.

The global weighted mean anomaly correlation between GRACE and the pseudo-observations for the total water storage is 0.43 (Figure 2b). The correlation is higher for the event regions in Russia (0.77), Europe (0.69), Midwest (0.52), and Australia (0.57). It is lower only for South Africa (0.39), where a negative trend is present in the pseudo-observations but not in GRACE (not shown). The pseudo-observations follow the temporal evolution of GRACE closely for 2010 in Russia (Figure 2d). The time series compare equally well for the other events/ regions (Text S2; Figure S5).

3.2. Single Events

We introduce each event by reviewing literature, and then we show the results for the experiments. Figures 3 and 4 display the spatial distribution and time series of anomalies in TX and SM, respectively, while Figure 5 summarizes the main response of the experiments during the selected 31 days.

3.2.1. The 2010 Russian Heat Wave

We examine the Russian heat wave 2010 over a region from 50°N to 60°N and 35°E to 55°E (black box in Figure 3, the same region as in Dole et al., 2011; Otto et al., 2012; Hauser et al., 2016). The event is characterized by a long period of extremely high temperatures as shown in Figure 3 for the anomalies of TX in ERA-Interim. The atmospheric feature associated with the heat wave was a persistent blocking anticyclone (e.g., Barriopedro et al., 2011; Otto et al., 2012; Trenberth & Fasullo, 2012). The heat wave was exacerbated by a lack of water available for evaporation, which resulted from early snow melt, a deficit of precipitation since the beginning of the year, and, as a consequence, decreasing SM (Barriopedro et al., 2011). Miralles et al. (2014) also point out the important indirect effects of the SM deficit, which are an enhanced entrainment of warm air during the day and the formation of a persistent warm residual layer above the atmospheric boundary layer during nighttime, where the heat can be stored and reenter the mixed layer the next day. Already in April and May SM in ERA-Land decreases to around -1.7σ (Figure 4), which aligns well with mild spring temperatures (Figure 3). After a short recovery in June the SM anomaly reaches about -3.5σ at the peak of the heat wave.

We focus on the period from 15 July to 14 August 2010, which is temporally centered on the largest temperature anomaly for the region and also shows large SM anomalies (maps in Figures 3 and 4). The average TX anomaly corresponds to almost 10°C above climatology in ERA-Interim and -3σ for SM in ERA-Land, as indicated by the black dashed lines in Figures 5a and 5b. Among the model estimates, those with nudged atmosphere get closest to the observed TX anomaly, which can be expected since they reproduce the blocking anticyclone (compare the height of the 500-hPa Geopotential in Figure S3a). aF_smF reproduces the TX anomaly in ERA-Interim quite well; however, it is too warm compared to Berkeley Earth (Figure 5a).

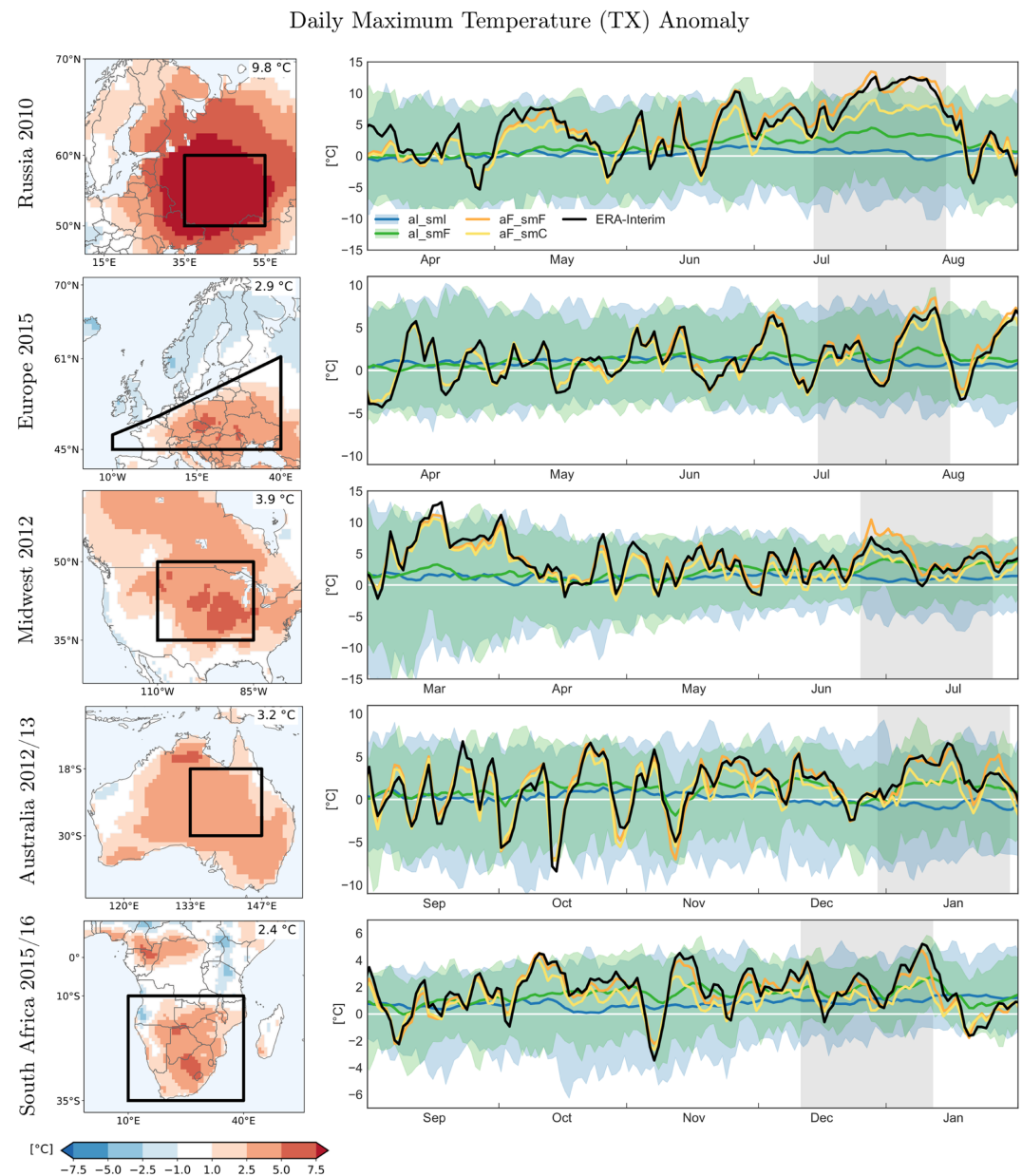


Figure 3. Daily maximum temperature (TX) for the five analyzed events. The maps to the left show the largest 31-day average anomaly of 2-m temperature for ERA-Interim, which was used to define the event. The black box shows the outline of the region investigated. The number in the upper right corner corresponds to the weighted average anomaly for the box. The time series to the right show the anomaly of TX compared to the 1982–2008 climatology for all experiments (line: ensemble mean; envelope: range) and for ERA-Interim (black line). The time period highlighted in gray shows the 31-day event period.

Prescribing SM to the climatology (aF_smC) decreases the TX anomaly by 35%. The anomaly for the experiment with only SM prescribed (aI_smF) is 32% of the anomaly in aF_smF . Both results indicate that SM plays a role in making this event as extreme as it was. For the aI_smI experiments there is a small positive TX anomaly for the ensemble mean. However, part of this anomaly is not due to the prescribed SSTs but attributable to the global temperature increase forced by GHGs. This effect is estimated by using the anomalies of $aI_smI_{2010-16}$. The best estimate for the increase in TX induced by recent climate change is roughly 1.2°C with nearly 75% of the members showing a positive anomaly. This suggests that the ocean-induced effect, that is, the effect of the SST pattern of 2010, is a cooling of -0.8°C (i.e., $aI_smI - aI_smI_{2010-16}$). However, large uncertainties are associated with these two estimates. Nevertheless, the result agrees with

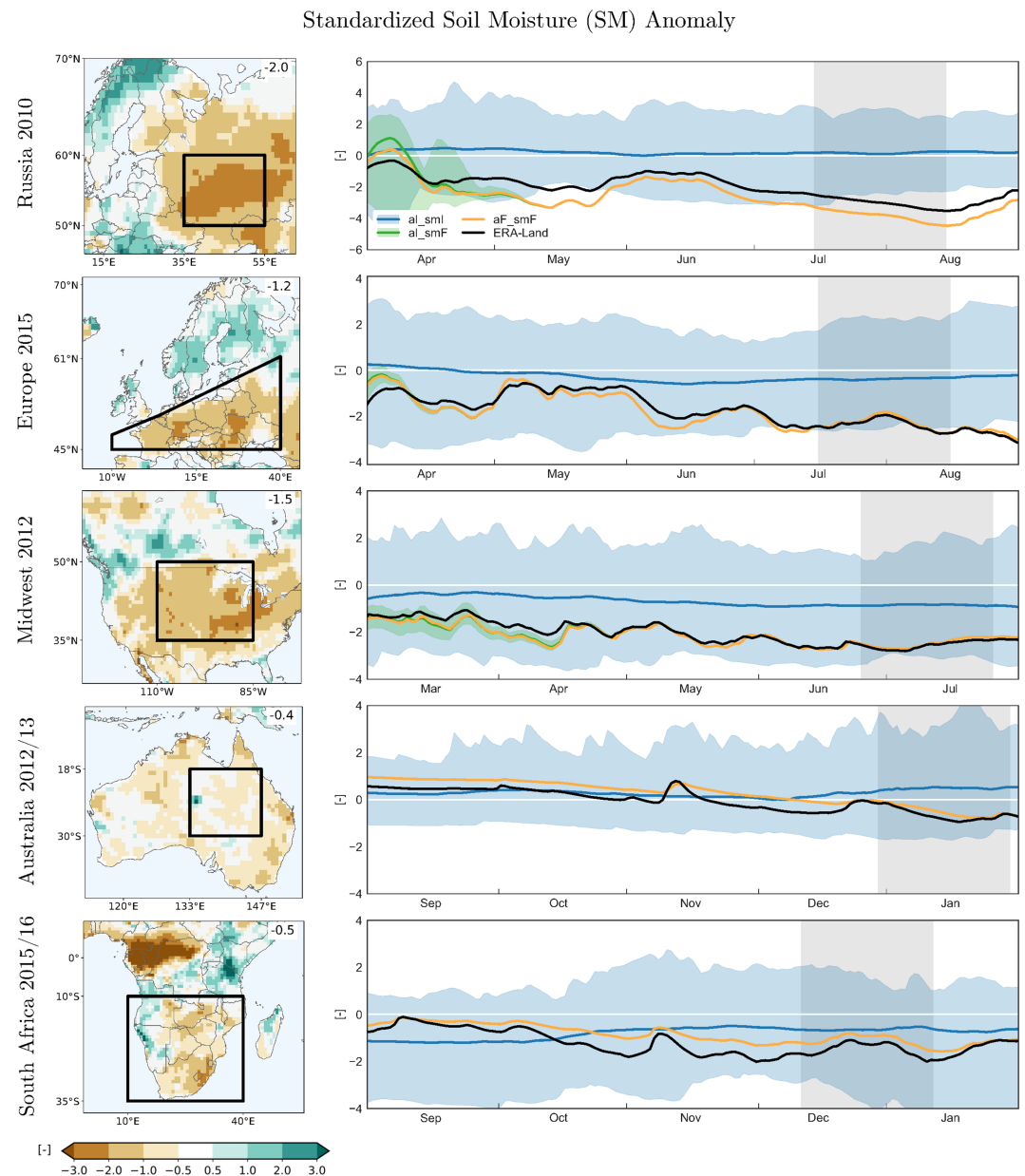


Figure 4. Same as Figure 3 but for standardized soil moisture (SM) in the upper 1 m. The reference for the time series is ERA-Land, which is also shown in the maps to the left. For the maps SM is standardized grid point wise, while for the time series we standardize for the region. We do not show the result for aF_smC as it is by definition always equal to 0. The green line (aI_smF) is mostly behind the orange line (aF_smF) as SM is prescribed to the same values in both experiments, except when (parts of) the soil is frozen.

the studies by Dole et al. (2011) and Hauser et al. (2016), which both found that the ocean forcing had no strong influence on the heat wave and the latter study even found a smaller heat wave risk for the 2010 ocean compared to other ocean states of the same decade.

The land surface in the experiments with SM prescription shows a larger dry anomaly than ERA-Land (Figure 5b). However, surface SM and total water storage change is well represented (Figures 2c and 2d). The anomalies of aI_smF and aF_smF are clearly outside the range encompassed by aI_smI (Figure 5b, compare also Figure 4). In aI_smI there is a small positive SM anomaly, which links to a positive precipitation anomaly (Figure 5c) and confirms that the ocean forcing was not favorable for a drought. The precipitation deficit in aF_smF (-1.33 mm/day) is smaller than in MSWEP (-1.63 mm/day), GPCC (-1.68 mm/day), or

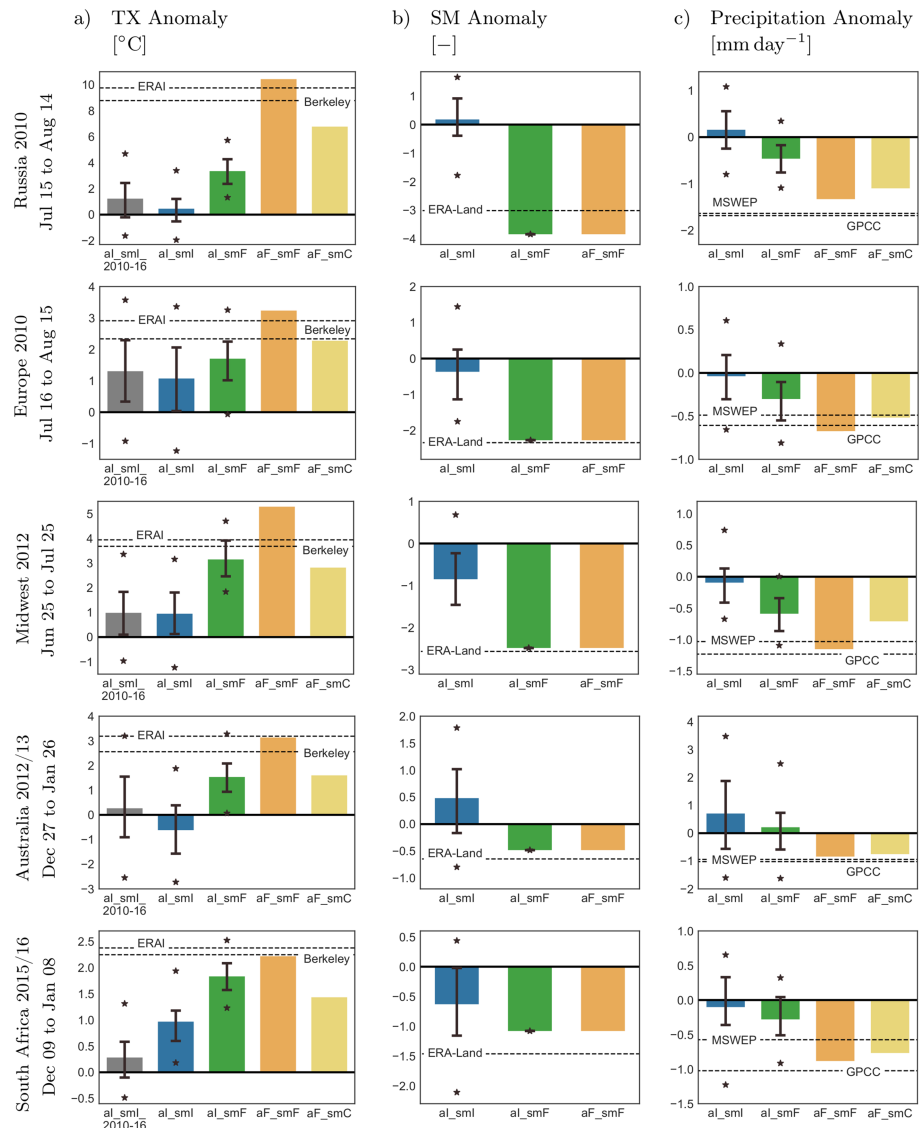


Figure 5. Regionally and temporally averaged anomalies for the five events analyzed. Shown are (a) daily maximum temperature (TX), (b) standardized soil moisture (SM), and (c) precipitation. The bars show the ensemble mean, the black line the 25th to 75th percentile, and the stars mark the 5th and 95th percentile values. The black dashed line indicates the value of the reference, which is ERA-Interim (ERA-I) as well as Berkeley Earth (Berkeley) for TX; ERA-Land for SM and GPCC as well as MSWEP for precipitation. *al_smI_2010-16* is shown for TX only because we use it to estimate the GHG contribution to TX. SM for *aF_smC* is not shown, as the anomaly is 0 by definition.

ERA-Interim (-2 mm/day, not shown). In percentages this corresponds to a reduction with respect to climatological precipitation of -71% for *aF_smF*, -85% for GPCC, -81% for MSWEP, and -84% for ERA-Interim. Nevertheless, the response in the model is sensitive enough to reproduce the anomaly in TX and SM.

High surface temperatures during heat waves can be driven by anomalies in radiative fluxes or surface turbulent fluxes. SW_{in} in the fully prescribed experiment (*aF_smF*) is well over the 95th percentile of *al_smI* (Figure S3b). This is attributable to the particular atmospheric circulation state, which favors subsiding air flow and inhibits cloud formation, thus leading to increased insolation of the land surface (Barriopedro et al., 2011). Compared to CERES, SW_{in} in *aF_smF* is too high (Figure S3b); however, it is close to ERA-Interim (not shown). EF is strongly reduced below climatological values (Figure S3c), which can result from increased SH or reduced LH or most likely both effects simultaneously. These anomalies in the surface turbulent fluxes are attributable to the negative SM anomaly and indicative of the drought conditions.

Literature on the 2010 Russian heat wave has identified the blocking anticyclone and the severe SM deficit as important drivers, while the ocean did not contribute to making the event more extreme. Our results lead us to the same conclusion. We demonstrate that while the atmospheric circulation did likely play the main role, the event anomaly was substantially enhanced due to the SM conditions.

3.2.2. The 2015 European Heat Wave

To examine the European summer of 2015, we choose the Central European (CEU) region, defined in the IPCC Special Report on Managing the Risks of Extreme Events and Disasters to Advance Climate Change Adaptation (SREX; Seneviratne et al., 2012). The 2015 heat wave was not a single event, but instead, four hot spells struck central continental Europe between the end of June and September (Sippel et al., 2016). A simultaneous precipitation deficit and concurrent drought led to a drying of the soil and intensified the event through land-atmosphere feedbacks (Dong et al., 2016; Hauser et al., 2017; Orth et al., 2016a). We examine the 31-day period from 16 July to 15 August, which encompasses two peaks of the summer heat wave interrupted by a few days of colder temperatures in the middle of the time period (Figure 3).

Due to the short and rainy (not shown) interruption of the heat wave in the middle of our event period, the average anomaly in TX is only about 2.9°C in ERA-Interim, 2.3°C in Berkeley Earth, and 3.2°C in *aF_smF* (Figure 5a). The daily maximum anomaly reached during the event period is about 7°C in ERA-Interim (Figure 3). *aF_smF* reproduces the temporal evolution of TX well and, however, overestimates the severity of the second peak. *aF_smC* reproduces 70% of the mean anomaly in *aF_smF* (Figure 5a) and follows the temporal evolution very accurately (Figure 3). This implies that the atmospheric circulation is a strong driver of the event. The average TX anomaly for *aI_smF* is about half of the anomaly in *aF_smF* (Figure 5a), which is a consequence of the temporal averaging over a time period with a cooling in the middle. The best estimate for the GHG-forced recent warming is about 1.3°C (interquartile range 0.3–2.3°C, *aI_smI_2010-16*). On average, *aI_smI* is a bit colder, and consequently, the contribution of the ocean anomaly of that year to the event is rather a very small cooling. This contradicts other hypotheses (e.g., Dong et al., 2016; Duchez et al., 2016) saying that the cold North Atlantic Ocean temperatures and strong meridional SST gradient might have been an important factor contributing to the heat wave. Whether this discrepancy is related to our framework or the employed model is outside the scope of this paper. If ocean-atmosphere coupling was important in this process, we might be unable to fully capture the impacts within a setup using prescribed SSTs. We conclude that within our framework there is a cooling signal of the ocean but that there are large uncertainties associated with this result. Even though there is a strong decrease in SM (Figures 5b and S5), this does not strongly affect the partitioning of the heat fluxes (EF for *aI_smI* and *aF_smF*; Figure S3c). This indicates that the contribution of the land surface to the TX anomaly in *aF_smF* is likely smaller than for the 2010 Russian heat wave. It might be due to the temporal averaging over 31 days and the rainy interruption during this time period that we cannot identify severe drought conditions.

In summary, the atmospheric circulation and the GHG forcing are key drivers of the European heat wave 2015 with a smaller but important effect of SM. Other studies on the event (e.g., Orth et al., 2016a) emphasize the role of SM deficit. Our results, however, indicate that SM had a smaller contribution than, for example, for the 2010 Russian heat wave. The role of the ocean is highly uncertain, and we find a weakly negative contribution.

3.2.3. The 2012 Midwest Heat Wave and Drought

In summer 2012 the Central Great Plains experienced a heat wave together with a severe drought, which was exceptional in terms of the area affected, its rapid development and the absence of early warning signs (Hoerling et al., 2014; Wang et al., 2014). The preceding winter and spring were characterized by unusually warm conditions, especially during March 2012 (Dole et al., 2014), which led to early snow cover retreat in the western and northern United States (PaiMazumder & Done, 2016; Wang et al., 2014). Already in 2011 the southern Plains—mainly Texas and Mexico—experienced a hot and dry summer, which was related to the La Niña conditions of 2010/2011 (Hoerling et al., 2013; Seager et al., 2014; Wang et al., 2014). However, dry conditions did not continue into the following year and the La Niña event had almost decayed (Hoerling et al., 2014; Wang et al., 2014). There are indications from model simulations (e.g., Schubert et al., 2009) and observations (Kushnir et al., 2010) that the United States summer climate is sensitive to forcing by the Atlantic, where indeed extraordinarily high SSTs occurred during 2012 (Hoerling et al., 2014). However, Wang et al. (2014) find the contribution from SST forcing to be small for the 2012 Midwest heat wave and drought and identify the atmospheric circulation as a main driver, which agrees with findings of

Hoerling et al. (2014). A series of high-pressure anomalies in the upper-troposphere inhibited cyclone activity in spring and thunderstorm formation during summer, which created positive temperature anomalies and an unprecedented deficit in rainfall (Hoerling et al., 2014; Wang et al., 2014). The drying of the soil further exacerbated the intensity of the heat wave through land-atmosphere interactions (AghaKouchak, 2014; PaiMazumder & Done, 2016; Wang et al., 2014). In the following, we focus on a region in the mid-western United States spanning 35°N to 50°N and 110°W to 55°W (the same region as in PaiMazumder & Done, 2016).

The most extreme temperatures are found during the first half of the event period, which is from 25 June to 25 July 2012, whereas during the second half there is only a moderate warm anomaly in TX (Figure 3). For the event period aF_smF overestimates the observed average anomaly in TX by more than 1°C (Figure 5a). This could be related to the surface turbulent fluxes, since the forced model shows too high values for SH and slightly too low values for LH in the climatological mean compared to GSWP-2 (Figure S1). It could also be related to biases in radiation that might be caused by erroneous cloud cover (Figure S3b). The TX anomaly for both $aI_smI_{2010-16}$ and aI_smI is about 1°C (Figure 5a), which indicates that there was a contribution from recent global warming (over 75% of the $aI_smI_{2010-16}$ members agree on the positive sign of the TX anomaly), but the ocean contribution is negligible, in agreement with Wang et al. (2014). Both aI_smF and aF_smC capture over half of the TX anomaly in aF_smF , which suggests a similarly important role of the atmospheric circulation and the land surface conditions. This is confirmed by the large anomalies for EF (Figure S3c) and SW_{in} (Figure S3b). For the SM anomaly there is a dry signal by the ocean (aI_smI , Figure 5b). However, the precipitation is only a bit below climatology on average (Figure 5c). Thus, the signal in SM is probably related to persisting dry conditions after the drought in 2011, where the ocean was a contributing factor (Wang et al., 2014). Whether such dry conditions were present in the region prior to the event is not consistent among different SM data sets. For ERA-Land we find an anomaly of around -1.5 to -2σ in spring (Figure 4) and around -2.6σ during the event (Figure 5b). Conversely, in ESA-CCI there is no anomaly until April (Figure S5). As our pseudo-observations for SM prescription are derived from ERA-Interim atmospheric forcing, which is also used to force ERA-Land, it is evident that our experiments behave similarly. Total water storage compares well for aF_smF and GRACE, showing drier-than-normal conditions starting from June for the model and from July for GRACE (Figure S5). AghaKouchak (2014) and PaiMazumder and Done (2016) find evidence for a role of pre-summer SM on the 2012 event, which is confirmed for root-zone SM (about 1-m depth) within our framework.

The results presented here suggest that SM and the atmospheric circulation were about equally important for the 2012 Midwest heat wave and drought. We find a small but nonnegligible contribution by global warming relative to the 1982–2008 climatology, but no strong effect of the 2012 SST patterns. In comparison, other studies identify the atmospheric circulation as a main driver of the event, and some also find a contribution of SM, while there is no consensus on the role of the ocean.

3.2.4. The 2012/2013 Australian Heat Wave and Drought

The summer of 2012/2013 in Australia was warmer than any summer before, with January 2013 being the hottest month on record at the time of the event (Bureau of Meteorology, 2013), surpassed only by January 2019 (Bureau of Meteorology, 2019). Earlier record summers such as in 1997/1998 were preceded by dry conditions caused by an El Niño event (Lewis & Karoly, 2013). In contrast, an extended La Niña event led to heavy rainfalls during 2010 to 2011 (Bureau of Meteorology, 2012), and SSTs in the equatorial Pacific Ocean were cool to neutral during the summer of 2012/2013 (NOAA Climate Prediction Center, 2019). Using climate models, Lewis and Karoly (2013) find a strong influence of GHG forcing and that natural variability alone would unlikely lead to the record event. Below-average rainfall had already occurred since July 2012 (Perkins et al., 2014) and strong correlations between precipitation and heat anomaly point to an important contribution of dry soils to the extreme summer (King et al., 2014). We focus on a region in eastern Australia from 18°S to 30°S and 133°E to 147°E (the same region as in King et al., 2014) and define the event period from 27 December 2012 to 26 January 2013.

Wetter-than-normal conditions of the 1-m soil column are seen before the event in September and October for ERA-Land and the model (Figure 4). This might be due to the La Niña conditions of the previous years, which would also agree with the experiment driven only by ocean conditions (aI_smI) having higher-than-average SM as well. From November to January model and observations show a drying of the soil. For the thin surface layer mostly drier-than-normal conditions are observed already from August on

(Figure S5). The TX anomaly during the event is close to ERA-Interim, however a bit overestimated compared to Berkeley Earth for the fully prescribed experiment (aF_smF , Figure 5a). Both aI_smF and aF_smC explain about one half of the temperature anomaly, which indicates an equally important contribution by atmospheric circulation and land surface conditions. There is a very small positive signal from recent GHG forcing ($aI_smI_{2010-16}$). aI_smI shows a negative TX anomaly, while SM and precipitation are above normal (Figures 5a–5c). This indicates that the contribution by the SSTs is unfavorable for the event, which is in line with the expected ENSO signal and with the findings of King et al. (2014). However, we do not find such a large contribution by GHGs as suggested by Lewis and Karoly (2013). This can be explained by the fact that they compare to conditions at the beginning of the 20th century while we only consider recent climate change and our climatology already includes climate change effects.

SW_{in} in aF_smF is anomalously high compared to aI_smI (Figure S3b), which results in anomalies of the radiative fluxes (Figure S3c) and drives surface temperature anomalies. However, SW_{in} in aF_smF is also underestimated compared to CERES (Figure S3b). Despite the relatively small SM anomaly, EF is strongly reduced (Figure S3c), which indicates that the region is experiencing drought conditions. The EF of aF_smC is considerably smaller than that of aI_smI . This is a consequence of the SM climatology being drier in the pseudo-observations compared to the model with interactive SM (Figure S2). Nevertheless, the dry anomaly during the event and the high evaporative demand lead to a further reduction of EF and increased surface temperature. Thus, the drought conditions were an important factor driving the extreme heat, which agrees with King et al. (2014). Additionally, we also find a strong contribution by the atmospheric circulation.

In summary, our results align with other studies showing that the ocean was no factor for the extreme summer in Australia and likely decreased its likelihood. Other studies identify a strong contribution of long-term climate change, which cannot be verified using our framework. We find that the atmospheric circulation and SM conditions play a roughly equally important role.

3.2.5. The 2015/2016 South African Heat Wave and Drought

The South Africa heat wave and drought of summer 2015/2016 is the most recent event examined in this study. The analysis is carried out over a region from 10°S to 35°S and 10°E to 40°E (same region as in Yuan et al., 2018). Sudden heat wave periods occurred during the rain season from November to April and led to the most extreme phase of the event in the beginning of December. Most parts of the region experienced concurrent drought conditions (Yuan et al., 2018). October to December 2015 was the peak of one of the strongest observed El Niño events, which lasted until spring 2016 (Iskandar et al., 2018). In an interplay with the SSTs in the Indian Pacific ocean, these conditions bring high-pressure anomalies and precipitation deficit to the southern part of the African continent (Hoell et al., 2015, 2017; Richard et al., 2000). Yuan et al. (2018) identify the high-pressure anomaly as a second important driver of the event, next to the SSTs, and show that it is positively correlated with temperature and negatively with precipitation. Indeed, an almost persistent high-pressure anomaly prevails during our event period and already during the previous weeks (not shown). The modeled average 500-hPa geopotential height for the event is not extremely anomalous as it lies just below the 95th percentile of the interactive atmosphere model (Figure S3a). Nevertheless, the persistence of the high-pressure anomaly some weeks ahead of the event can lead to the observed accumulation of heat and suppression of precipitation. We define the event period from 9 December 2015 to 8 January 2016, where the highest temperature anomaly of the summer (Figure 3) and a moderate SM deficit were observed (Figure 4).

The observed TX anomaly is well captured in aF_smF (Figure 5a). aI_smF can reproduce almost the entire TX anomaly in aF_smF (83% on average; Figure 5a). The TX anomaly explained by aF_smC is 65% of aF_smF , which is, however, not much more than explained by aI_smI on average. This suggests that land-atmosphere feedbacks and SM preconditions had a more important role than atmospheric dynamics. The contribution from recent GHG forcing is a warming of about 0.3°C and consequently the ocean contribution is a warming of another 0.7°C in the mean. There is a dry SM signal during the event in aI_smI (Figure 5b; 75% of the members agree on the sign), which can be due to the SST patterns, the conditions prior to the event, and due to recent climate change.

Similarly to the 2012/2013 summer in Australia, SW_{in} is strongly increased in aF_smF compared to aI_smI , but it is still underestimated compared to CERES (Figure S3b). Also, there is a strong decrease of EF for aI_smF and aF_smF , despite a moderate SM anomaly compared to the other events (Figures 5b and

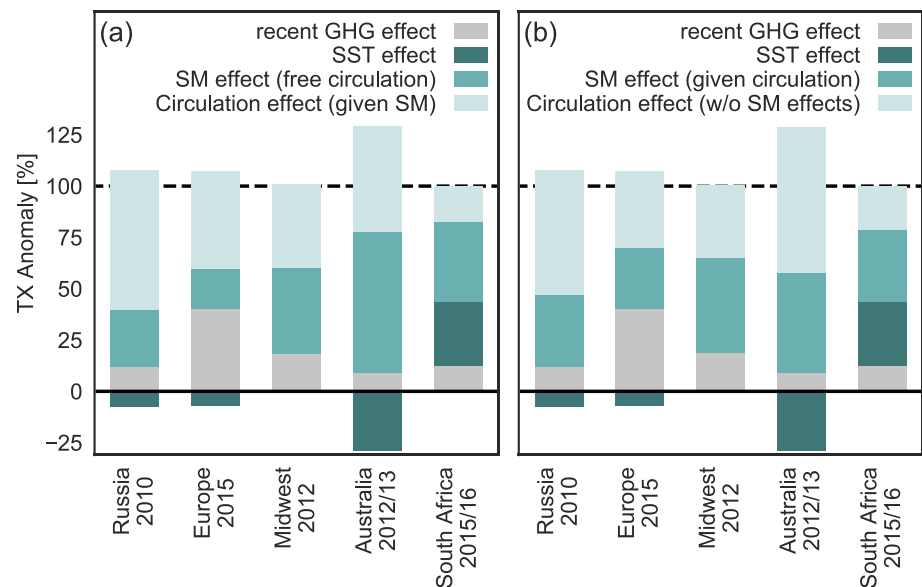


Figure 6. Contribution of the physical drivers and climate change to the TX anomaly. The individual contributions are normalized by the modeled TX anomaly in aF_smF . Shown are two approaches to separate SM effects from atmospheric circulation effects: (a) the SM effect with free atmospheric circulation ($aI_smF - aI_smI$) and the atmospheric circulation effect given the observed SM ($aF_smF - aI_smF$); (b) the atmospheric circulation effect without induced SM effects ($aF_smC - aI_smI$) and the SM effect given the observed circulation ($aF_smF - aF_smC$). Not shown are the uncertainty ranges of the estimates for the SM effect with free circulation, the GHG effect, and the effect of SSTs on the event year.

S3c). Together, this points to a high contribution of the land surface conditions but also some influence of atmospheric dynamics to the extreme heat.

Overall, our results support the conclusions by Yuan et al. (2018) that the SSTs were an important driver of the 2015/2016 South African heat wave and drought. Additionally, we identify a strong effect of the SM preconditions. The role of atmospheric circulation is likely linked to ocean-atmosphere feedback processes (due to the strong El Niño event). Persistent anticyclonic conditions were important to prolong the heat and drought during the event period. Initially, however, the preconditions given by land and ocean were crucial to bring about the event.

3.3. Synthesis of the Physical Processes Throughout Events

In the previous section we have discussed qualitatively which processes were the most important drivers for each of the extreme events investigated. In the following, we give a quantitative estimate for the role of each driver by analyzing its contribution to the TX anomaly during the event, in the model. The recent GHG effect is estimated from $aI_smI_{2010-16}$, and the contributions of the other factors are computed from the differences between the experiments as described in section 2.6. The results are summarized in Figure 6. It is noteworthy that the two approaches to estimate the SM and atmospheric circulation contributions give quite similar results, providing confidence in our framework. For the 2010 Russian heat wave the best estimate for the recent GHG forcing signal explains around 10% of the event anomaly. The ocean has a small negative contribution, while the rest of the TX anomaly can be attributed to atmospheric circulation and SM conditions in a 70:30 ratio for approach A and roughly 60:40 for approach B. The 2015 European heat wave has the largest climate change signal of all investigated events, explaining 40% of the event anomaly. The ocean has again a small negative contribution. The contribution of the atmospheric circulation is larger than that of SM with a ratio of nearly 60:40 for approach A and 70:30 for approach B. For the 2012 Midwest heat wave and drought, the GHG forcing explains nearly 20% of the anomaly while the ocean contribution is below 1%. The ratios between circulation and SM are 50:50 for approach A and 40:60 for approach B. The 2012/2013 Australian heat wave and drought shows a strong negative ocean contribution while the GHG forcing was about 9%. SM dominates the TX anomaly for approach A with a ratio of 40:60, but the circulation contribution is larger for approach B with the opposite ratio (60:40). The 2015/2016 South African heat wave and drought is the only event investigated with a positive ocean contribution, explaining 30% of

the total anomaly. The GHG forcing explains around 13%. For both approaches the role of the atmospheric circulation is less important compared to SM with the ratios being 30:70 and 40:60 for approaches A and B, respectively. Note that these estimates are specific to the event and region investigated; that is, the “same” event in another region might result from other drivers, and other events in the same region might result from a different combination of the drivers.

Considering all analyzed events, atmospheric circulation and SM play similarly important roles, each contributing around 20–70% to the total events’ anomalies. The ocean contribution is generally small, except for the 2015/2016 South African heat wave and drought and the 2012/2013 Australian heat wave and drought, which were both driven by El Niño teleconnections. Recent climate change explains about 10–20% of the anomalies. For the 2015 European heat wave, however, the recent GHG contribution is considerably larger, suggesting a strong climate change signal for TX in that region, relative to the 1982–2008 climatology. The results are qualitatively the same when repeating the analysis using a 15-day event period (Figure S6).

The majority of the investigated events is located in regions that are known as SM-temperature coupling hot spots. Especially for the Midwestern United States, South Africa, and Australia, a strong land-atmosphere coupling is found (Miralles et al., 2012; Seneviratne et al., 2006). These regions are located in transitional climate zones where evapotranspiration (and thus latent cooling) is strongly dependent on SM availability. This might explain why we find the highest SM contribution to TX for the three events in these regions. Depending on the method and data set used, a medium to strong coupling is also identified for the Mediterranean and Eastern Europe (Seneviratne et al., 2010, 2006).

4. Conclusions

This study was motivated by the recent occurrence of extreme heat waves in different regions of the globe. We investigate the heat waves of 2010 in Russia, 2012 in the Midwest, 2012/2013 in Australia, 2015 in Europe, and 2015/2016 in South Africa. To isolate the role of the physical processes, we perform factorial experiments with the Earth System Model CESM, in which the atmospheric flow and/or land surface conditions are forced toward observations. The large-scale atmospheric circulation is prescribed using atmospheric nudging. Previous studies on nudging found a reliable adjustment of the atmospheric circulation with the underlying climatology of the other variables in the model not being fundamentally affected (Lin et al., 2016; Wehrli et al., 2018; Zhang et al., 2014). Thus, climatological biases remain after introducing nudging, which was also found for CESM (Wehrli et al., 2018). We demonstrate that the nudged simulations can accurately reproduce the observed anomalies of extreme heat waves. This result indicates that there might be benefits from bias correction for the simulation of observed events and possibly also for the projection of future extreme events.

The role of the physical drivers of the five heat waves discussed is summarized in Figure 6. Relative to the reference climatology of 1982–2008, we find a positive contribution of recent climate change on TX for all investigated events. The estimates range between 0.3 and 1.3°C, for a global mean temperature increase of 0.3°C in the model. However, the signal is not uniform for all ensemble members due to climate variability. The biggest role of recent GHG forcing is found for the 2015 European heat wave, where it is a main driver of the event. Similarly to the global warming signal, the contribution from the ocean conditions is highly variable. We only see a strong signal for the 2012/2013 Australian heat wave and drought and for the 2015/2016 South African heat wave and drought. For the latter the ocean forcing explains nearly a third of the event magnitude, whereas for Australia the SSTs induced adverse conditions for the event. Both effects are in line with the expected ENSO signal for the two regions (Hoell et al., 2017, 2015; Power et al., 1999). Thus, the ocean is a bigger factor for regions that are close to the coast and experience teleconnections from ENSO.

The largest part of the events’ anomalies is explained by atmospheric circulation, SM, or a combination of the two. We find that atmospheric circulation was the key driver of the 2010 Russian heat wave, while SM had the biggest contribution to those heat waves that occurred simultaneously with extreme droughts, that is, the ones in 2012 in the Midwest, 2012/2013 in Australia, and 2015/2016 in South Africa. For the 2012/2013 event in Australia either the circulation or SM is more important, depending on how the contributions are computed. For all events, except Australia 2012/2013, we find a negative SM anomaly several months before the heat wave in the observations as well as in the model. Hence, the preconditioning of the land surface is an important factor. This is a result of the land-atmosphere coupling: SM is a response to earlier conditions

of the atmospheric circulation and can then have an effect on circulation through modifying mesoscale circulation, convection, radiation, cloud cover, boundary layer stability, and planetary wave structures (Guillod et al., 2015; Koster et al., 2014; Santanello et al., 2018; Seneviratne et al., 2010; Taylor et al., 2011; Vogel et al., 2018). This highlights the importance of an accurate representation of the land within weather prediction. Unfortunately, land surface models employed in weather prediction often lag behind current state of the art and also behind their atmospheric counterparts (Davin et al., 2016). Actions to be taken may include improving the initialization of the land surface (e.g., Ardilouze et al., 2017; Koster et al., 2010; Prodhomme et al., 2016) and implementing a better representation of land surface processes (e.g., Davin et al., 2016; Orth et al., 2016b; Santanello et al., 2015).

Our framework allows us to disentangle the contributions of different physical drivers to the heat waves, but it also has limitations. Ideally, one would consider all feedback loops to understand each extreme event. This is not possible in our conditional framework as feedback on components that are prescribed is missing. Similarly, all experiments are run with prescribed SSTs; thus, ocean-atmosphere interactions cannot evolve. It was shown that ensembles from such prescribed ocean experiments display less variability, for example, of surface temperature compared to coupled experiments (Fischer et al., 2018). Another characteristic of the nudged simulations is that atmospheric variability is strongly reduced within the nudged ensembles, which does not allow to use probabilistic approaches such as risk ratios. Some of this latter problem is overcome by following two different approaches to estimate the role of circulation versus that of the land surface. Further, by computing differences to a fully forced model simulation, we assume that the effects we study are additive. The two different approaches show that this is probably not fully accurate, although this appears to be overall a reasonable approximation. Another caveat arises from the difference in the SM climatologies of the experiments with and without SM prescription. This is overcome by using anomalies instead of absolute values in the analysis. Nonetheless, the differences in the SM climatologies might trigger a different response to the same SM anomaly (e.g., if different SM regimes are reached). Also, we only estimate the influence of recent climate change given by the anomaly compared to a 1982–2008 climatology. Lastly, we use a rather simplistic approach to disentangle the contributions from SSTs and climate change. Despite these drawbacks, our conditional approach provides insights in the qualitative role of the specific drivers.

In this study we quantify the role of the recent GHG forcing, ocean, atmospheric circulation, and SM for five recent heat waves. We introduce a new experimental framework for disentangling the driving processes of extreme events. This framework is shown to provide valuable mechanistic insight and information on the causalities of the investigated events. While some events are mainly driven by global warming and the atmospheric circulation, other events are identified where SM plays a key role with a contribution of up to 70% of the events' anomalies. This highlights that the role of the thermodynamics can be just as important as that of the dynamics for temperature extremes, a possibly underestimated feature. On the other hand, SSTs were found to play a minor to negligible role for the considered events, except in South Africa and Australia. It would be useful to confirm the robustness of this result with a multimodel assessment. In conclusion, this study highlights the combined role of thermodynamical and dynamical processes affecting heat extremes in midlatitudes and the value of assessing these separate contributions in a changing climate.

References

- AghaKouchak, A. (2014). A baseline probabilistic drought forecasting framework using standardized soil moisture index: application to the 2012 United States drought. *Hydrology and Earth System Sciences*, 18(7), 2485–2492.
- Arblaster, J. M., Lim, E.-P., Hendon, H. H., Trewin, B. C., Wheeler, M. C., Liu, G., & Braganza, K. (2014). Understanding Australia's hottest September on record. *Bulletin of the American Meteorological Society*, 95, 37–41.
- Ardilouze, C., Batté, L., Bunzel, F., Decremier, D., Déqué, M., Doblas-Reyes, F. J., & Prodhomme, C. (2017). Multi-model assessment of the impact of soil moisture initialization on mid-latitude summer predictability. *Climate Dynamics*, 49(11), 3959–3974.
- Balsamo, G., Albergel, C., Beljaars, A., Boussetta, S., Brun, E., Cloke, H., et al. (2015). ERA-Interim/Land: A global land surface reanalysis data set. *Hydrology and Earth System Sciences*, 19(1), 389–407.
- Barriopedro, D., Fischer, E. M., Luterbacher, J., Trigo, R. M., & García-Herrera, R. (2011). The hot summer of 2010: Redrawing the temperature record map of Europe. *Science*, 332(6026), 220–224.
- Beck, H. E., Wood, E. F., Pan, M., Fisher, C. K., Miralles, D. G., van Dijk, A. I., & Adler, R. F. (2018). MSWEP V2 global 3-hourly 0.1° precipitation: Methodology and quantitative assessment. *Bulletin of the American Meteorological Society*, 100, 473–500. <https://doi.org/10.1175/BAMS-D-17-0138.1>
- Brönnimann, S. (2007). Impact of El Niño–Southern Oscillation on European climate. *Reviews of Geophysics*, 45, RG3003. <https://doi.org/10.1029/2006RG000199>
- Bureau of Meteorology (2012). Australia's wettest two-year period on record; 2010–2011. Spec. Clim. Statement, 38 (available through: <http://www.bom.gov.au/climate/current/statements/scs38.pdf>).

Acknowledgments

We thank two anonymous reviewers for their constructive feedback on our manuscript. This work was carried out within the European Research Council (ERC) 'DROUGHT-HEAT' project (Grant 617518) funded by the European Community's Seventh Framework Programme. The ERA-Interim reanalysis data sets are available from the ECMWF website (<http://www.ecmwf.int/en/research/climate-reanalysis/era-interim>). Berkeley Earth Data is available from the Berkeley Earth website (<http://berkeleyearth.org/data>). For MSWEP we use Version 2.2 that can be obtained online (from <http://www.gloh2o.org/>). The daily full data product 2018 of GPCC can be obtained from DWD (at <http://gpcc.dwd.de/>). CERES v4a data were obtained from the NASA Langley Research Center Atmospheric Science Data Center (<https://ceres.larc.nasa.gov/products.php?product=SYN1deg>). The combined soil moisture data product from ESA-CCI is available from the ESA-CCI Soil Moisture website (<https://www.esa-soilmoisture-cci.org/>). GRACE Mascon data are available online (at <http://grace.jpl.nasa.gov/>), supported by the NASA MEASURES Program. The data underlying the presented research can be downloaded from the ETH Research Collection under the Creative Commons Attribution 4.0 International license (doi: 10.3929/ethz-b-000349923). We acknowledge Emanuel Dutra and ECMWF for providing the ERA-Interim/Land extension to 2018 without precipitation correction; the data are available at the ECMWF data archive as research experiment identification gd6e. We thank Vincent Humphrey for support with the use of GRACE data.

- Bureau of Meteorology (2013). Extreme heat in January 2013. Spec. Clim. Statement 43 (available through: <http://www.bom.gov.au/climate/current/statements/scs43e.pdf>).
- Bureau of Meteorology (2019). Widespread heatwaves during December 2018 and January 2019. Spec. Clim. Statement 68 (available through: <http://www.bom.gov.au/climate/current/statements/scs68.pdf>).
- Davin, E. L., Maisonnave, E., & Seneviratne, S. I. (2016). Is land surface processes representation a possible weak link in current Regional Climate Models? *Environmental Research Letters*, 11(7), 074027.
- de Jeu, R. A. M., Wagner, W., Holmes, T. R. H., Dolman, A. J., van de Giesen, N. C., & Friesen, J. (2008). Global soil moisture patterns observed by space borne microwave radiometers and scatterometers. *Surveys in Geophysics*, 29(4), 399–420.
- Dee, D. P., Uppala, S. M., Simmons, A. J., Berrisford, P., Poli, P., Kobayashi, S., et al. (2011). The ERA-Interim reanalysis: Configuration and performance of the data assimilation system. *Quarterly Journal of the Royal Meteorological Society*, 137(656), 553–597.
- Deo, R. C., Syktus, J. I., McAlpine, C. A., Lawrence, P. J., McGowan, H. A., & Phinn, S. R. (2009). Impact of historical land cover change on daily indices of climate extremes including droughts in eastern Australia. *Geophysical Research Letters*, 36, L08705. <https://doi.org/10.1029/2009GL037666>
- Dirmeyer, P. A., Gao, X., Zhao, M., Guo, Z., Oki, T., & Hanasaki, N. (2006). GSWP-2: Multimodel analysis and implications for our perception of the land surface. *Bulletin of the American Meteorological Society*, 87(10), 1381–1398.
- Dlugokencky, E. (2018). NOAA/ESRL. www.esrl.noaa.gov/gmd/ccgg/trends_ch4/, accessed 14 February 2018.
- Dlugokencky, E., & Tans, P. (2018). NOAA/ESRL. www.esrl.noaa.gov/gmd/ccgg/trends/, accessed 14 February 2018.
- Doelling, D. (2017). CERES Level 3 SYN1DEG-DAYTerra+Aqua HDF4 file - Edition 4A [Data set]. NASA Langley Atmospheric Science Data Center DAAC, https://doi.org/10.5067/terra+aqua/ceres/syn1degday_l3.004a
- Dole, R., Hoerling, M., Kumar, A., Eischeid, J., Perlwitz, J., Quan, X.-W., et al. (2014). The making of an extreme event: Putting the pieces together. *Bulletin of the American Meteorological Society*, 95(3), 427–440.
- Dole, R., Hoerling, M., Perlwitz, J., Eischeid, J., Pegion, P., Zhang, T., et al. (2011). Was there a basis for anticipating the 2010 Russian heat wave? *Geophysical Research Letters*, 38, L06702. <https://doi.org/10.1029/2010GL046582>
- Donat, M. G., Alexander, L. V., Yang, H., Durrie, I., Vose, R., Dunn, R. J. H., et al. (2013). Updated analyses of temperature and precipitation extreme indices since the beginning of the twentieth century: The HadEX2 dataset. *Journal of Geophysical Research: Atmospheres*, 118, 2098–2118. <https://doi.org/10.1002/jgrd.50150>
- Dong, B., Sutton, R., Shaffrey, L., & Wilcox, L. (2016). The 2015 European heat wave. *Bulletin of the American Meteorological Society*, 97(12), S57–S62.
- Dorigo, W. A., Wagner, W., Albergel, C., Albrecht, F., Balsamo, G., Brocca, L., & Lecomte, P. (2017). ESA CCI soil moisture for improved Earth system understanding: State-of-the art and future directions. *Remote Sensing of Environment*, 203, 185–215.
- Duchez, A., Frajka-Williams, E., Josey, S. A., Evans, D. G., Grist, J. P., Marsh, R., & Hirschi, J. J.-M. (2016). Drivers of exceptionally cold North Atlantic Ocean temperatures and their link to the 2015 European heat wave. *Environmental Research Letters*, 11(7), 074004.
- Fischer, E. M., Beyerle, U., Schleussner, C. F., King, A. D., & Knutti, R. (2018). Biased estimates of changes in climate extremes from prescribed SST simulations. *Geophysical Research Letters*, 45, 8500–8509. <https://doi.org/10.1029/2018GL079176>
- Fischer, E. M., & Knutti, R. (2015). Anthropogenic contribution to global occurrence of heavy-precipitation and high-temperature extremes. *Nature Climate Change*, 5(6), 560–564.
- Fischer, E. M., Seneviratne, S. I., Vidale, P. L., Lüthi, D., & Schär, C. (2007). Soil moisture-atmosphere interactions during the 2003 European Summer Heat Wave. *Journal of Climate*, 20(20), 5081–5099.
- Gruber, A., Dorigo, W. A., Crow, W., & Wagner, W. (2017). Triple collocation based merging of satellite soil moisture retrievals. *IEEE Transactions on Geoscience and Remote Sensing*, 55(12), 6780–6792.
- Guillod, B. P., Orłowsky, B., Miralles, D. G., Teuling, A. J., & Seneviratne, S. I. (2015). Reconciling spatial and temporal soil moisture effects on afternoon rainfall. *Nature Communications*, 6, 6443.
- Hauser, M., Gudmundsson, L., Orth, R., Jézéquel, A., Hausteine, K., Vautard, R., et al. (2017). Methods and model dependency of extreme event attribution: The 2015 European drought. *Earth's Future*, 5, 1034–1043. <https://doi.org/10.1002/2017EF000612>
- Hauser, M., Orth, R., & Seneviratne, S. I. (2016). Role of soil moisture versus recent climate change for the 2010 heat wave in western Russia. *Geophysical Research Letters*, 43, 2819–2826. <https://doi.org/10.1002/2016GL068036>
- Hauser, M., Orth, R., & Seneviratne, S. I. (2017). Investigating soil moisture-climate interactions with prescribed soil moisture experiments: An assessment with the Community Earth System Model (version 1.2). *Geoscientific Model Development*, 10(4), 1665–1677.
- Hirschi, M., Seneviratne, S. I., Alexandrov, V., Boberg, F., Boroneant, C., Christensen, O. B., & Stepanek, P. (2011). Observational evidence for soil-moisture impact on hot extremes in southeastern Europe. *Nature Geoscience*, 4(1), 17–21.
- Hoell, A., Funk, C., Magadzire, T., Zinke, J., & Husak, G. (2015). El Niño-Southern Oscillation diversity and Southern Africa teleconnections during austral summer. *Climate Dynamics*, 45(5), 1583–1599.
- Hoell, A., Funk, C., Zinke, J., & Harrison, L. (2017). Modulation of the Southern Africa precipitation response to the El Niño Southern Oscillation by the subtropical Indian Ocean Dipole. *Climate Dynamics*, 48(7), 2529–2540.
- Hoerling, M., Eischeid, J., Kumar, A., Leung, R., Mariotti, A., Mo, K., et al. (2014). Causes and predictability of the 2012 Great Plains drought. *Bulletin of the American Meteorological Society*, 95(2), 269–282.
- Hoerling, M., Kumar, A., Dole, R., Nielsen-Gammon, J. W., Eischeid, J., Perlwitz, J., et al. (2013). Anatomy of an extreme event. *Journal of Climate*, 26(9), 2811–2832.
- Hope, P., Lim, E.-P., Wang, G., Hendon, H. H., & Arblaster, J. M. (2015). Bulletin of the American Meteorological Society. *Bulletin of the American Meteorological Society*, 96(12), 149–153.
- Hope, P., Wang, G., Lim, E.-P., Hendon, H. H., & Arblaster, J. M. (2016). What caused the record-breaking heat across Australia in October 2015? *Bulletin of the American Meteorological Society*, 97(12), S122–S126.
- Hurrell, J. W., Hack, J. J., Shea, D., Caron, J. M., & Rosinski, J. (2008). A new sea surface temperature and sea ice boundary dataset for the Community Atmosphere Model. *Journal of Climate*, 21(19), 5145–5153.
- Hurrell, J. W., Holland, M. M., Gent, P. R., Ghan, S., Kay, J. E., Kushner, P. J., et al. (2013). The Community Earth System Model: A framework for collaborative research. *Bulletin of the American Meteorological Society*, 94(9), 1339–1360.
- Iskandar, I., Lestari, D., Utari, P., Sari, Q., Setiabudidaya, D., Mardiansyah, W., et al. (2018). How strong was the 2015/2016 El Niño event? *Journal of Physics: Conference Series*, 1011(1), 012030.
- Jaeger, E. B., & Seneviratne, S. I. (2011). Impact of soil moisture-atmosphere coupling on European climate extremes and trends in a regional climate model. *Climate Dynamics*, 36(9), 1919–1939.
- Jeuken, A. B. M., Siegmund, P. C., Heijboer, L. C., Feichter, J., & Bengtsson, L. (1996). On the potential of assimilating meteorological analyses in a global climate model for the purpose of model validation. *Journal of Geophysical Research*, 101(D12), 16939–16950.

- Kay, J. E., Deser, C., Phillips, A., Mai, A., Hannay, C., Strand, G., et al. (2015). The Community Earth System Model (CESM) large ensemble project: A community resource for studying climate change in the presence of internal climate variability. *Bulletin of the American Meteorological Society*, 96(8), 1333–1349.
- King, A. D., Karoly, D. J., Donat, M. G., & Alexander, L. V. (2014). Climate change turns Australia's 2013 big dry into a year of record-breaking heat in "Explaining Extremes of 2013 from a Climate Perspective". *Bulletin of the American Meteorological Society*, 95(9), 41–45.
- Koopman, G. J., Pritchard, M. S., Ghan, S. J., Wang, M., Somerville, R. C. J., & Russell, L. M. (2012). Constraining the influence of natural variability to improve estimates of global aerosol indirect effects in a nudged version of the Community Atmosphere Model 5. *Journal of Geophysical Research*, 117, D23204. <https://doi.org/10.1029/2012JD018588>
- Koster, R. D., Chang, Y., & Schubert, S. D. (2014). A mechanism for land-atmosphere feedback involving planetary wave structures. *Journal of Climate*, 27(24), 9290–9301.
- Koster, R. D., Dirmeyer, P. A., Guo, Z., Bonan, G., Chan, E., Cox, P., et al. (2004). Regions of strong coupling between soil moisture and precipitation. *Science*, 305(5687), 1138–1140. PubMed-not-MEDLINE.
- Koster, R. D., Guo, Z., Yang, R., Dirmeyer, P. A., Mitchell, K., & Puma, M. J. (2009). On the nature of soil moisture in land surface models. *Journal of Climate*, 22(16), 4322–4335.
- Koster, R. D., Mahanama, S. P. P., Yamada, T. J., Balsamo, G., Berg, A. A., Boisserie, M., & Wood, E. F. (2010). Contribution of land surface initialization to subseasonal forecast skill: First results from a multi-model experiment. *Geophysical Research Letters*, 37, L02402. <https://doi.org/10.1029/2009GL041677>
- Kushnir, Y., Seager, R., Ting, M., Naik, N., & Nakamura, J. (2010). Mechanisms of Tropical Atlantic SST influence on North American precipitation variability. *Journal of Climate*, 23(21), 5610–5628.
- Lawrence, D. M., Oleson, K. W., Flanner, M. G., Thornton, P. E., Swenson, S. C., Lawrence, P. J., & Slater, A. G. (2011). Parameterization improvements and functional and structural advances in version 4 of the Community Land Model. *Journal of Advances in Modeling Earth Systems*, 3, M03001. <https://doi.org/10.1029/2011MS00045>
- Lejeune, Q., Davin, E. L., Gudmundsson, L., Winckler, J., & Seneviratne, S. I. (2018). Historical deforestation locally increased the intensity of hot days in northern mid-latitudes. *Nature Climate Change*, 8(5), 386–390.
- Lewis, S. C., & Karoly, D. J. (2013). Anthropogenic contributions to Australia's record summer temperatures of 2013. *Geophysical Research Letters*, 40, 3705–3709. <https://doi.org/10.1002/grl.50673>
- Lim, E.-P., Hendon, H. H., Arblaster, J. M., Chung, C., Moise, A. F., Hope, P., & Zhao, M. (2016). Interaction of the recent 50 year SST trend and La Niña 2010: Amplification of the Southern Annular Mode and Australian springtime rainfall. *Climate Dynamics*, 47(7), 2273–2291.
- Lin, G., Wan, H., Zhang, K., Qian, Y., & Ghan, S. J. (2016). Can nudging be used to quantify model sensitivities in precipitation and cloud forcing? *Journal of Advances in Modeling Earth Systems*, 8, 1073–1091. <https://doi.org/10.1002/2016MS000659>
- Liu, Y. Y., Dorigo, W. A., Parinussa, R. M., de Jeu, R. A. M., Wagner, W., McCabe, M. F., & van Dijk, A. I. (2012). Trend-preserving blending of passive and active microwave soil moisture retrievals. *Remote Sensing of Environment*, 123, 280–297.
- Lorenz, R., Jaeger, E. B., & Seneviratne, S. I. (2010). Persistence of heat waves and its link to soil moisture memory. *Geophysical Research Letters*, 37, L09703. <https://doi.org/10.1029/2010GL042764>
- Matthes, K., Funke, B., Andersson, M. E., Barnard, L., Beer, J., Charbonneau, P., & Versick, S. (2017). Solar forcing for CMIP6 (v3.2). *Geoscientific Model Development*, 10(6), 2247–2302. <https://doi.org/10.5194/gmd-10-2247-2017>
- Meehl, G. A., & Tebaldi, C. (2004). More intense, more frequent, and longer lasting heat waves in the 21st century. *Science*, 305(5686), 994–997.
- Miralles, D. G., Teuling, A. J., van Heerwaarden, C. C., & Vila-Guerau de Arellano, J. (2014). Mega-heatwave temperatures due to combined soil desiccation and atmospheric heat accumulation. *Nature Geoscience*, 7(5), 345–349.
- Miralles, D. G., van den Berg, M. J., Teuling, A. J., & de Jeu, R. A. M. (2012). Soil moisture-temperature coupling: A multiscale observational analysis. *Geophysical Research Letters*, 39, L21707. <https://doi.org/10.1029/2012GL053703>
- Mueller, B., & Seneviratne, S. I. (2012). Hot days induced by precipitation deficits at the global scale. *Proceedings of the National Academy of Sciences*, 109(31), 12398–12403.
- NOAA Climate Prediction Center (2019). Historical El Niño/La Niña episodes (1950-present) based on the Oceanic Niño Index. https://origin.cpc.ncep.noaa.gov/products/analysis_monitoring/ensostuff/ONI_v5.php, accessed 12 June 2019.
- NOAA Earth System Research Laboratory (2018). Combined nitrous oxide data from the NOAA/ESRL Global Monitoring Division. ftp://ftp.cmdl.noaa.gov/hats/n2o/combined/HATS_global_N2O.txt, accessed 14 February 2018.
- Neale, R. B., Chen, C.-C., Gettelman, A., Lauritzen, P. H., Park, S., Williamson, D. L., & Taylor, M. A. (2012). Description of the NCAR Community Atmosphere Model (CAM 5.0) (Technical Report). Boulder, Colorado: National Center for Atmospheric Research.
- Oleson, K. W., Lawrence, D. M., Bonan, G. B., Flanner, M. G., Kluzek, E., Lawrence, P. J., & Zeng, X. (2010). Technical description of version 4.0 of the Community Land Model (CLM) (Technical Report). Boulder, Colorado: National Center for Atmospheric Research.
- Orth, R., Dutra, E., & Pappenberger, F. (2016b). Improving weather predictability by including land surface model parameter uncertainty. *Monthly Weather Review*, 144(4), 1551–1569.
- Orth, R., Zscheischler, J., & Seneviratne, S. I. (2016a). Record dry summer in 2015 challenges precipitation projections in Central Europe. *Scientific Reports*, 6, 28334.
- Otto, F. E. L., Massey, N., van Oldenborgh, G. J., Jones, R. G., & Allen, M. R. (2012). Reconciling two approaches to attribution of the 2010 Russian heat wave. *Geophysical Research Letters*, 39, L04702. <https://doi.org/10.1029/2011GL050422>
- PaiMazumder, D., & Done, J. M. (2016). Potential predictability sources of the 2012 U.S. drought in observations and a regional model ensemble. *Journal of Geophysical Research: Atmospheres*, 121, 12,581–12,592. <https://doi.org/10.1002/2016JD025322>
- Parker, T. J., Berry, G. J., & Reeder, M. J. (2014). The structure and evolution of heat waves in southeastern Australia. *Journal of Climate*, 27(15), 5768–5785.
- Perkins, S. E., Lewis, S. C., King, A. D., & Alexander, L. V. (2014). Increased simulated risk of the hot Australian summer of 2012/13 due to anthropogenic activity as measured by heat wave frequency and intensity. *Bulletin of the American Meteorological Society*, 95, 34–37.
- Pfahl, S., & Wernli, H. (2012). Quantifying the relevance of atmospheric blocking for co-located temperature extremes in the Northern Hemisphere on (sub-)daily time scales. *Geophysical Research Letters*, 39. <https://doi.org/10.1029/2012GL052261>
- Power, S. B., Casey, T., Folland, C., Colman, A., & Mehta, V. (1999). Inter-decadal modulation of the impact of ENSO on Australia. *Climate Dynamics*, 15(5), 319–324.
- Power, S. B., & Delage, F. P. D. (2019). Setting and smashing extreme temperature records over the coming century. *Nature Climate Change*, 9(7), 529–534.
- Prodhomme, C., Doblas-Reyes, F., Bellprat, O., & Dutra, E. (2016). Impact of land-surface initialization on sub-seasonal to seasonal forecasts over Europe. *Climate Dynamics*, 47(3), 919–935.

- Quinting, J. F., & Reeder, M. J. (2017). Southeastern Australian heat waves from a trajectory viewpoint. *Monthly Weather Review*, 145(10), 4109–4125.
- Richard, Y., Trzaska, S., Roucou, P., & Rouault, M. (2000). Modification of the southern African rainfall variability/ENSO relationship since the late 1960s. *Climate Dynamics*, 16(12), 883–895.
- Rodríguez-Fernández, N. J., Kerr, Y. H., Van der Schalie, R., Al-Yaari, A., Wigneron, J.-P., De Jeu, R., et al. (2016). Long term global surface soil moisture fields using an SMOS-trained neural network applied to AMSR-E data. *Remote Sensing*, 8(11), 959.
- Rohde, R., Muller, R. A., Jacobsen, R., Muller, E., Perlmutter, S., Rosenfeld, A., et al. (2013). A new estimate of average Earth surface land temperature spanning 1743 to 2011. *Geoinformatics & Geostatistics: An Overview*, 1(1), 1–7.
- Rohde, R., Muller, R. A., Jacobsen, R., Perlmutter, S., Rosenfeld, A., Wurtele, J., et al. (2013). Berkeley Earth temperature averaging process. *Geoinformatics & Geostatistics: An Overview*, 1(2), 1–13.
- Ropelewski, C. F., & Halpert, M. S. (1987). Global and regional scale precipitation patterns associated with the El Niño/Southern Oscillation. *Monthly Weather Review*, 115(8), 1606–1626.
- Santanello, J. A., Dirmeyer, P. A., Ferguson, C. R., Findell, K. L., Tawfik, A. B., Berg, A., et al. (2018). Land-atmosphere interactions: The LoCo perspective. *Bulletin of the American Meteorological Society*, 99(6), 1253–1272.
- Santanello, J. A., Roundy, J., & Dirmeyer, P. A. (2015). Quantifying the land atmosphere coupling behavior in modern reanalysis products over the U.S. Southern Great Plains. *Journal of Climate*, 28(14), 5813–5829.
- Schaller, N., Kay, A. L., Lamb, R., Massey, N. R., van Oldenborgh, G. J., Otto, F. E. L., & Allen, M. R. (2016). Human influence on climate in the 2014 southern England winter floods and their impacts. *Nature Climate Change*, 6(6), 627–634.
- Schubert, S. D., Gutzler, D., Wang, H., Dai, A., Delworth, T., Deser, C., & Zeng, N. (2009). A U.S. CLIVAR project to assess and compare the responses of global climate models to drought-related SST forcing patterns: Overview and results. *Journal of Climate*, 22(19), 5251–5272.
- Schubert, S. D., Wang, H., Koster, R. D., Suarez, M. J., & Groisman, P. Y. (2014). Northern Eurasian heat waves and droughts. *Journal of Climate*, 27(9), 3169–3207.
- Seager, R., Goddard, L., Nakamura, J., Henderson, N., & Lee, D. E. (2014). Dynamical causes of the 2010/11 Texas-Northern Mexico drought. *Journal of Hydrometeorology*, 15(1), 39–68.
- Seneviratne, S. I., Corti, T., Davin, E. L., Hirschi, M., Jaeger, E. B., Lehner, I., et al. (2010). Investigating soil moisture-climate interactions in a changing climate: A review. *Earth-Science Reviews*, 99(3–4), 125–161.
- Seneviratne, S. I., Luthi, D., Litschi, M., & Schar, C. (2006). Land-atmosphere coupling and climate change in Europe. *Nature*, 443(7108), 205–209.
- Seneviratne, S. I., Nicholls, N., Easterling, D., Goodess, C. M., Kanae, S., Kossin, J., et al. (2012). Changes in climate extremes and their impacts on the natural physical environment. In C. B. Field (Ed.), *Managing the risks of extreme events and disasters to advance climate change adaptation*. Cambridge: Cambridge University Press, pp. 109–230.
- Seneviratne, S. I., Wilhelm, M., Stanelle, T., van den Hurk, B., Hagemann, S., Berg, A., & Smith, B. (2013). Impact of soil moisture-climate feedbacks on CMIP5 projections: First results from the GLACE-CMIP5 experiment. *Geophysical Research Letters*, 40, 5212–5217. <https://doi.org/10.1002/grl.50956>
- Shepherd, T. G. (2016). A common framework for approaches to Extreme Event Attribution. *Current Climate Change Reports*, 2(1), 28–38.
- Sippel, S., E. L. Otto, F., Flach, M., & Van Oldenborgh, G. J. (2016). The role of anthropogenic warming in 2015 Central European heat waves. *Bulletin of the American Meteorological Society*, 97, S51–S56.
- Stott, P. A., Stone, D. A., & Allen, M. R. (2004). Human contribution to the European heatwave of 2003. *Nature*, 432(7017), 610–614.
- Su, H., Neelin, J. D., & Chou, C. (2001). Tropical teleconnection and local response to SST anomalies during the 1997–1998 El Niño. *Journal of Geophysical Research*, 106, 20025–20043.
- Taylor, C. M., Gounou, A., Guichard, F., Harris, P. P., Ellis, R. J., Couvreur, F., & De Kauwe, M. (2011). Frequency of Sahelian storm initiation enhanced over mesoscale soil-moisture patterns. *Nature Geosci*, 4(7), 430–433.
- Thiery, W., Davin, E. L., Lawrence, D. M., Hirsch, A. L., Hauser, M., & Seneviratne, S. I. (2017). Present-day irrigation mitigates heat extremes. *Journal of Geophysical Research: Atmospheres*, 122, 1403–1422. <https://doi.org/10.1002/2016JD025740>
- Trenberth, K. E., & Fasullo, J. T. (2012). Climate extremes and climate change: The Russian heat wave and other climate extremes of 2010. *Journal of Geophysical Research*, 117, D17103. <https://doi.org/10.1029/2011JD018020>
- Trenberth, K. E., Fasullo, J. T., & Shepherd, T. G. (2015). Attribution of climate extreme events. *Nature Climate Change*, 5, 725–730.
- van Vuuren, D. P., Edmonds, J., Kainuma, M., Riahi, K., Thomson, A., Hibbard, K., & Rose, S. K. (2011). The representative concentration pathways: An overview. *Climatic Change*, 109(1), 5.
- Vogel, M. M., Orth, R., Cheruy, F., Hagemann, S., Lorenz, R., van den Hurk, B. J. J. M., & Seneviratne, S. I. (2017). Regional amplification of projected changes in extreme temperatures strongly controlled by soil moisture temperature feedbacks. *Geophysical Research Letters*, 44, 1511–1519. <https://doi.org/10.5194/esd-9-1107-2018>
- Vogel, M. M., Zscheischler, J., & Seneviratne, S. I. (2018). Varying soil moisture-atmosphere feedbacks explain divergent temperature extremes and precipitation projections in central Europe. *Earth System Dynamics*, 9(3), 1107–1125.
- Wang, G., Hope, P., Lim, E.-P., Hendon, H. H., & Arblaster, J. M. (2016). Three methods for the attribution of extreme weather and climate events (018): Bureau of Meteorology.
- Wang, H., Schubert, S., Koster, R., Ham, Y.-G., & Suarez, M. (2014). On the role of SST forcing in the 2011 and 2012 extreme U.S. heat and drought: A study in contrasts. *Journal of Hydrometeorology*, 15(3), 1255–1273.
- Watkins, M. M., Wiese, D. N., Yuan, D.-N., Boening, C., & Landerer, F. W. (2015). Improved methods for observing Earth's time variable mass distribution with GRACE using spherical cap mascons. *Journal of Geophysical Research: Solid Earth*, 120, 2648–2671. <https://doi.org/10.1002/2014JB011547>
- Weedon, G. P., Balsamo, G., Bellouin, N., Gomes, S., Best, M., & Viterbo, P. (2014). The WFDEI meteorological forcing data set: WATCH forcing data methodology applied to ERA-Interim reanalysis data. *Water Resources Research*, 50, 7505–7514. <https://doi.org/10.1002/2014wr015638>
- Weedon, G. P., Gomes, S., Viterbo, P., Shuttleworth, W. J., Blyth, E., Österle, H., & Best, M. (2011). Creation of the WATCH forcing data and its use to assess global and regional reference crop evaporation over land during the Twentieth Century. *Journal of Hydrometeorology*, 12(5), 823–848.
- Wehrli, K., Guillod, B. P., Hauser, M., Leclair, M., & Seneviratne, S. I. (2018). Assessing the dynamic versus thermodynamic origin of climate model biases. *Geophysical Research Letters*, 45, 8471–8479. <https://doi.org/10.1029/2018GL079220>
- Wiese, D. N., Landerer, F. W., & Watkins, M. M. (2016). Quantifying and reducing leakage errors in the JPL RL05M GRACE mascon solution. *Water Resources Research*, 52, 7490–7502. <https://doi.org/10.1002/2016WR019344>

- Wiese, D. N., Yuan, D.-N., Boening, C., Landerer, F. W., & Watkins, M. M. (2018). JPL GRACE mascon ocean, ice, and hydrology equivalent water height release 06 coastal resolution improvement (CRI) filtered version 1.0. Ver 1.0. PO.DAAC, CA, USA. <https://doi.org/10.5067/TEMSC-3MJC6>
- Yuan, X., Wang, L., & Wood, E. F. (2018). Anthropogenic intensification of Southern African flash droughts as exemplified by the 2015/16 season. *Bulletin of the American Meteorological Society*, 99(1), 86–90.
- Zhang, K., Wan, H., Liu, X., Ghan, S. J., Kooperman, G. J., Ma, P.-L., et al. (2014). Technical note: On the use of nudging for aerosol-climate model intercomparison studies. *Atmospheric Chemistry and Physics*, 14(16), 8631–8645.
- Ziese, M., Rauthe-Schöch, A., Becker, A., Finger, P., Meyer-Christoffer, A., & Schneider, U. (2018). GPCC Full Data Daily Version.2018 at 1.0° : Daily land-surface precipitation from rain-gauges built on GTS-based and historic data. Global Precipitation Climatology Centre (GPCC) at Deutscher Wetterdienst, https://doi.org/10.5676/dwd\ignorespacesgpcc/fd_d_v2018_100
- Zscheischler, J., & Seneviratne, S. I. (2017). Dependence of drivers affects risks associated with compound events. *Science Advances*, 3(6), e1700263.

Erratum

In the originally published version of this article, due to a typesetting error the arrows beneath “circulation effect” and “SM effect” in Figure 1B were incorrectly placed. The figure has since been corrected, and this version may be considered the authoritative version of record.